

Article

Electron Ionization of Size-Selected Positively and Negatively Charged Helium Droplets

Felix Laimer , Fabio Zappa , Elisabeth Gruber  and Paul Scheier 

Institut für Ionenphysik und Angewandte Physik, Universität Innsbruck, Technikerstr. 25, A-6020 Innsbruck, Austria; fabio.zappa@uibk.ac.at (F.Z.); e.gruber@uibk.ac.at (E.G.)

* Correspondence: felix.laimer@uibk.ac.at (F.L.); paul.scheier@uibk.ac.at (P.S.); Tel.: +43-512-507-52660 (P.S.)

Abstract: A beam of size-selected charged helium droplets was crossed with an electron beam, and the ion efficiency curves for the product droplets in all different charge states were recorded. We estimate that the selected helium droplets on their passage through the electron beam are hit by several hundred electrons which can interact with the individual He atoms of the droplets. Reaction channels corresponding to the removal or capture of up to eight electrons were identified, and in all cases, inelastic scattering and the formation of metastable helium played a significant role.

Keywords: electron ionization; electron capture; helium droplets; cross section



Citation: Laimer, F.; Zappa, F.; Gruber, E.; Scheier, P. Electron Ionization of Size-Selected Positively and Negatively Charged Helium Droplets. *Atoms* **2021**, *9*, 74. <https://doi.org/10.3390/atoms9040074>

Academic Editor: Grzegorz Piotr Karwasz

Received: 31 August 2021

Accepted: 30 September 2021

Published: 5 October 2021

Publisher's Note: MDPI stays neutral with regard to jurisdictional claims in published maps and institutional affiliations.



Copyright: © 2021 by the authors. Licensee MDPI, Basel, Switzerland. This article is an open access article distributed under the terms and conditions of the Creative Commons Attribution (CC BY) license (<https://creativecommons.org/licenses/by/4.0/>).

1. Introduction

Ionization, neutralization, and fragmentation of ions upon electron impact are fundamental processes in natural and technical plasmas [1,2]. Cross sections can be calculated, for instance, by utilizing the semiclassical Deutsch–Märk formalism [3] or the binary-encounter-dipole theory [4,5]. For H_2^+ , the electron ionization cross sections were determined by full quantum calculations [6], and excellent agreement was found with the experimental values [7]. The experimental determination of cross sections of ionic targets is a challenging task, and only very few instruments have been designed for this purpose. The groups of Defrance and Salzborn independently developed a method to obtain absolute cross sections by determining the overlap geometry between the ion beam and the electron beam by scanning the electron beam through the ion beam either mechanically [8] or with a pair of deflector plates [9,10]. Dolder and Peart obtained the overlap by moving an aperture through the region where the ion and electron beam overlap [11]. The electron impact on large molecular target ions was investigated for fullerene cations by Matt et al. [12], who reported an increase in the charge state with and without fragmentation. The group of Salzborn extended these studies and determined the absolute cross sections for positively and negatively charged fullerene ions [13,14]. To our knowledge, no data are available for larger clusters.

Helium droplets have been investigated since their first production by Becker and coworkers in 1961 [15], but it took almost 30 years until the scientific community became aware of their full potential. With the discovery that helium droplets are able to capture atoms [16] and molecules [17], the formation of clusters and complexes [16,18] and the spectroscopy of cold molecules in the most inert matrix were achieved [17,19]. Aside from optical spectroscopy of neutral dopants [20–23], mass spectrometry of charged products formed via various ionization techniques is a commonly utilized method [24–27]. The high excitation and ionization energy of helium requires rather advanced light sources and makes electron guns simple alternatives that are frequently utilized. Mass spectra obtained upon electron ionization of undoped helium droplets are dominated by small helium cluster ions of the form He_n^+ . According to the literature, these cluster ions are predominantly formed via electron ionization of a He atom and subsequent resonant hole hopping toward the center of the droplet [28–30]. After typically 11 hops, vibrationally

excited He_2^+ is formed that is either ejected from the droplet or becomes solvated by polarized neighboring He atoms and thereby forming a so-called Atkins snowball [31]. Mateo and Eloranta determined from electronic structure calculations a linear He_3^+ ionic core of such snowballs [32]. However, since positively charged ions are strongly heliophilic, the mass spectrometric observation of small helium cluster ions implies that these have to be ejected from large droplets or are the residue from the evaporation of small, charged helium droplets. Based on the binding energy of He_2^+ , the internal energy of vibrationally excited He_2^+ is able to vaporize only 3500 He atoms at most. Thus, a different mechanism such as Coulomb repulsion between more than one charged species is required to explain the ejection of low-mass ions from larger He droplets.

Recently, Laimer et al. discovered that both the positive [33] and negative ionization [34] of helium droplets, aside from the low-mass ions often recorded in mass spectrometers, also leads to the formation of a massive, charged residual droplet that contains the majority of the mass of the neutral precursor. In fact, the mass loss due to evaporation of neutral He atoms and ejection of low-mass ions is negligible for droplets containing several million He atoms. In both studies, neutral helium droplets were ionized via electron bombardment. Then, a first spherical sector electrostatic energy analyzer selected a narrow slice from the charged droplet distribution, and these droplets were bombarded by a second electron beam. A second energy analyzer was used to analyze the mass per charge values of the final product droplets and investigate the arrangement of charge centers. Furthermore, these droplets can become highly charged, with appearance sizes for multiply charged droplets being more than an order of magnitude larger for anionic droplets [34].

In the present paper, we investigate in detail the processes that lead to a change in the charged state of large differently charged helium droplets upon electron bombardment. Ion efficiency curves are measured in the electron energy range between 0 eV and 120 eV for all possible charged product ions formed upon electron bombardment of the mass per charge of selected helium droplets, utilizing a tandem set-up consisting of an electron ionization source followed by an electrostatic energy analyzer. The underlying mechanisms that are involved in changes in the charge state are identified by analyzing the positions of the resonances and the thresholds of the corresponding processes for individual charge states. In the case of positively charged helium droplets, an increase in the charge state preferentially proceeds at electron energies higher than 25 eV, whereas a reduction in the charge state happens at two narrow resonances of 2 eV and 22 eV, which can be assigned to electron attachment and the formation of intermediate He^{*-} , respectively.

2. Materials and Methods

Neutral He droplets were formed via expansion of He gas (99.9999% purity, Messer Austria GmbH, Gumpoldskirchen, Austria) with a stagnation pressure of 2 MPa through a pinhole nozzle with a diameter of 5 μm (A0200P, Plano GmbH, Wezlar, Germany) attached to an oxygen-free copper block (MB-OF101 with a residual-resistance ratio, RRR > 200, Montanwerke Brixlegg, Brixlegg, Austria) that was mounted to the second stage of a closed-circuit cryocooler (RDK-408D2, Sumitomo Heavy Industries Ltd., Tokyo, Japan). Through a combination of the cooling by the cryocooler and resistive heating, we were able to control the temperature of the compressed He down to 4.2 K. In the present investigation, temperatures of 7 K and 9 K were selected, and 11.7 mm downstream from the nozzle, the droplets passed through a skimmer with an aperture of 0.8 mm on their way into the first ionization source. Here, the droplets were ionized by the impact of electrons with a kinetic energy of 40 eV and an electron current of 300 μA for promoting the formation of positively charged droplets and 30 eV and 430 μA for negatively charged droplets. The ionizer design was based on a Nier-type electron source using a tungsten coil filament. Charged droplets were then mass-per-charge selected by a spherical sector electrostatic 90° energy analyzer with a central radius of 7 cm and a distance between the plates of 2 cm. The resolving power of the two energy analyzers was limited by the apertures and was determined from the width and position of the precursor peaks to $E/\Delta E \sim 63$. The m/z -

selected charged droplets could then be ionized further by a second electron ionization source of the same type as the first one. A second electrostatic analyzer identical to the first one was then employed to analyze the final mass-per-charge ratio of the droplets, which were detected with a Channeltron-type secondary electron multiplier (Dr. Sjuts, KBL 510). The energy resolution when measuring electron energy-dependent ion efficiency curves was estimated by analyzing the signal decrease for the cationic precursor peak signal around 22 eV. A Gaussian fit on the derivative of the slope gave an upper limit of ± 0.65 eV for the spread in electron energy. A residual gas pressure of about 10^{-6} Pa was achieved with turbomolecular pumps (one HiPace 2300, two HiPace 700 and one TMU 521, Pfeiffer Vacuum Technology AG, Aßlar, Germany) backed by two oil-free roughing pumps (ACP 40, Pfeiffer Vacuum Technology AG, Aßlar, Germany). A schematic diagram of the apparatus is shown in Figure 1.

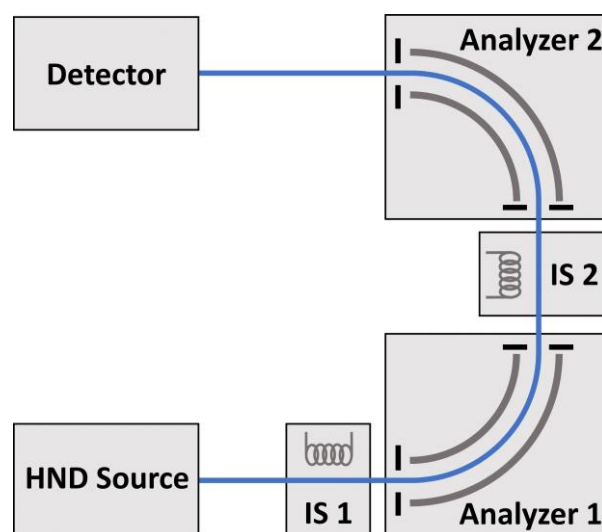


Figure 1. Schematic of the experimental set-up.

The velocity distributions at different nozzle temperatures of the droplet beam were measured recently by Laimer et al. via a time-of-flight method by pulsing the electron energy [35]. The velocities of the singly charged He droplets of the selected precursor mass-per-charge-values at 7 K and 9 K ranged from $v = 155$ to 169 m/s and 196 m/s, respectively. The kinetic energy of a charged droplet passing the electrostatic energy analyzer could be determined from the electric field E applied and its central radius, with the mass-per-charge value of the droplet being equivalent to $2E/v^2$.

3. Results and Discussion

3.1. Penetration Depth of the Electrons in the He Droplets

The high density and large size of He droplets lead to non-uniform ionization and excitation probability of the He atoms inside. Using Beer's law, the density of liquid helium (0.02 \AA^{-3} [36]) and the cross sections for electron ionization and excitation of helium atoms [37], the penetration depth of electrons can be determined as a function of their kinetic energy. Figure 2 shows the distance at which the electron current is attenuated to $1/e = 37\%$. The horizontal line indicates the diameter of a He droplet containing 5.7 million He atoms. The vertical line corresponds to the ionization energy of He. For droplets of this size, metastable He formation at collision energies around 22 eV can be expected to happen throughout the volume of the droplet, whereas electron ionization is preferentially happening close to the surface and facing the impinging electron beam.

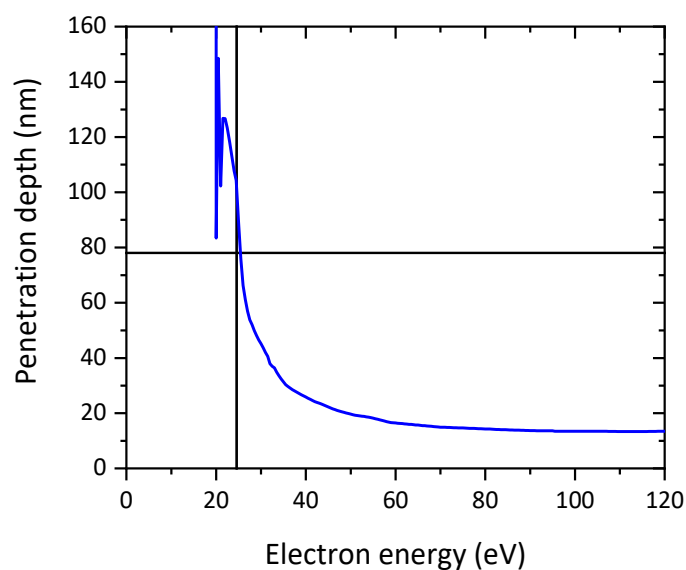


Figure 2. Penetration depth of electrons in liquid helium, determined from Beer’s law using the bulk density of He and the cross sections for electron excitation and ionization. The horizontal line indicates the diameter of a He droplet containing 5.7 million He atoms, and the vertical line indicates the ionization energy of He.

3.2. Cations to Cations

Positively charged He droplets were formed upon electron bombardment of neutral He droplets (expansion conditions of 7 K and 2 MPa, average neutral droplet size of 1.1×10^7 [38]) with an electron energy of 40 eV and an electron current of $300 \mu\text{A}$. This results in a log-normal-shaped m/z distribution with an average value of about 7 million He atoms per charge [35]. The first energy filter (Analyzer 1 in Figure 1) selected a narrow slice of this distribution at a relative m/z of 2.7×10^6 He atoms per charge (corresponding to a relative m/z value of 1 in Figure 3). In the second ion source (IS 2 in Figure 1), the selected droplets were crossed with a $210\text{-}\mu\text{A}$ electron beam, and depending on the electron energy, differently charged product droplets were formed. At 22 eV (blue line in Figure 3), most product droplets had higher m/z values than the selected precursor, thus indicating a reduction of the charge state. Peaks at the exact fractional numbers demonstrated negligible mass loss due to evaporation of neutral He atoms, as was already observed previously [33]. At 120 eV, an increase in the charge state resulted in lower m/z values (purple line in Figure 3). The presence of differently charged precursor droplets and a relatively poor energy resolution of the energy analyzer resulted in a curve where only the most intense product channels could be seen as narrow peaks at fractional number m/z values, such as $1/4$, $1/3$, $1/2$, $2/3$ and $3/4$. By setting the second ion source to 80 eV and $100 \mu\text{A}$, the formation of very highly charged droplets was strongly reduced, which enabled a better assignment of individual reaction channels (red line).

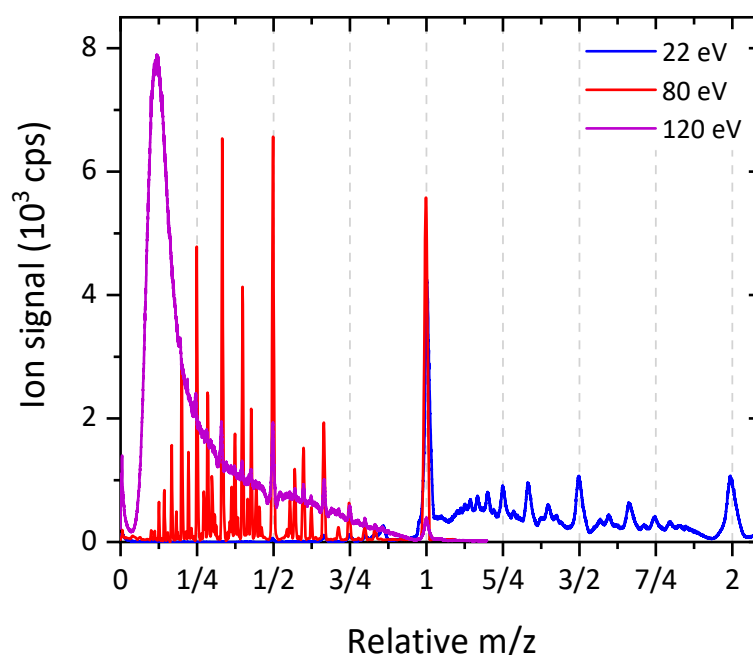


Figure 3. Charge distributions of positively charged He droplets resulting from electron bombardment of mass-per-charge selected positively charged He droplets containing 2.7×10^6 He atoms per charge. Electron energy of 22.5 eV resulted predominantly in a reduction in the charge state (blue line), whereas 120 eV (purple line) increased the charge state and led to a pile-up of peaks at a relative m/z value of 0.11 or 3×10^5 He atoms per charge. The red line was measured with the second ion source set to 80 eV and a reduced current of 100 μA .

3.2.1. Ion Efficiency Curves

The ion efficiency curves of all major product charge states were measured, recording the ion yield at the corresponding relative m/z values as a function of the electron energy of the second ion source from 0 eV to 120 eV. For a selected mass-per-charge value of 5.7 million He atoms per charge, most reaction channels that led to an increase in the charge state are plotted in Figure 4. The corresponding reaction channels found at relative m/z values lower than one are plotted in Figure 3. The curve labels are ordered according to the ratio of the initial and final charge states of the droplets. Reactions with z_i/z_f close to one (yellow to red lines) exhibited an asymmetric peak structure with a maximum at around 30 eV, followed by a minimum at 10 eV and a gentle increase up to 120 eV. Additionally, reaction channels with much lower z_i/z_f values (blue to purple lines) exhibited a relatively narrow peak-like shape quite different to typical electron ionization cross sections of atoms and small molecules. A similar resonance-like behavior was previously observed for the partial cross sections of fragment ions of fullerenes [39]. In that case, with increasing electron energy, neutral C_2 loss transforms larger product ions into smaller ones, resulting in narrow, peak-like cross section curves. In the present case, the removal of an additional electron at higher electron energies became more likely and thereby led to a decrease in the ion yield of lower-charged species and, at the same time, an increase in the signal of higher-charged product droplets.

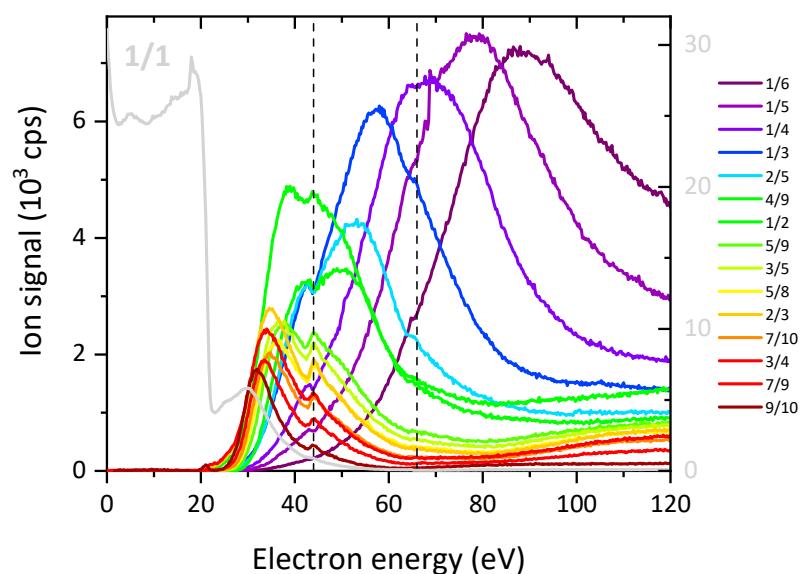
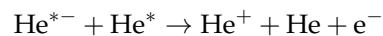


Figure 4. Ion efficiency curves for electron ionization of positively charged He droplets with a mass-per-charge ratio of 5.7 million He atoms per charge. The curves' labels are sorted according to the ratio of the precursor to final charge state, which is equivalent to the relative m/z values of the corresponding peaks in Figure 3. Note the two pronounced anomalies in the ion signal of several curves around 44 eV and 66 eV, designated by vertical dashed lines.

Since the first energy analyzer only selected the mass per charge, the peak at a relative $m/z = 1/2$ corresponded to singly charged He droplets containing 5.7 million He atoms that became doubly charged. However, it would also contain the signal from reactions where multiply charged droplets with an initial charge state z_i containing z_i times 5.7 million He atoms were ionized into a final charge state of $z_f = 2z_i$. The reaction channel that did not lead to a change in the charge state (designated as 1/1, the light gray line) is plotted with its corresponding y-axis drawn at the right side of the diagram. Both the maxima and threshold energies of the curves shifted to higher electron energies with decreasing z_i/z_f values. In addition, several curves exhibit pronounced peaks and wiggles at around 44 eV and 66 eV. These peaks match the resonances reported by Mauracher et al. [40], where He^{*-} and He_2^{*-} were efficiently formed and ejected from undoped He droplets. Ion efficiency curves for two other initial m/z values are shown in the Supplementary Materials (Figures S1 and S2). Droplet formation at 9 K resulted in neutral droplets that contained on average 4 million He atoms [38]. Thus, the contribution of multiply charged droplets at a selected m/z value of 4×10^6 , for instance, was substantially lower than in the case of the same selected m/z values when the He source was operated at a temperature of 7 K. This led to better separation of the peaks at lower relative m/z values. The appearance energy values for three different mass-per-charge values selected by the first analyzer (the ion efficiency curves for two data sets obtained for 2.7 and 4 million He atoms per charge are shown in the Supplementary Materials in Figures S1 and S2) were obtained by utilizing the vanishing current method for all curves where a well-defined final charge state was distinguishable. All appearance energies obtained by this method possessed an error of ± 1 eV introduced by a background signal. The results are listed in the Supplementary Materials in Table S1 and plotted in Figure 5 as a function of the difference of the final and initial charge states $z_f - z_i$. Despite the significant uncertainty in the determination of threshold values, it is apparent that all reaction channels followed the same trend, and it is remarkable that the threshold values for the reactions $+1 \rightarrow +5$ and $+5 \rightarrow +9$ were almost identical, albeit with a five times higher initial charge state for the latter process. The linear fit to the data in Figure 5 gave a value of 19.83 eV for $z_f - z_i = 0$, which is almost exactly the excitation energy of a He atom into the metastable 2^3S state. The slope of the linear fit in Figure 5 is 1.66 eV. The cross section of a He droplet containing $N > 10^4$ He

atoms was $4\pi r^2$, with $r = 0.22 \times N^{1/3}$. Thus, a droplet containing 5.7 million He atoms had a geometric cross section of 19,400 nm². The electron beam had a diameter of about 1 mm and a current of 300 μ A. During the passage of such a droplet through the electron beam, which took about 6.5 μ s (1 mm/155 m/s), we could estimate that this droplet would be hit by 234 electrons. The threshold energy required for multiple ionization would be determined by the most energetic process that one of these electrons had to drive. The energy of 19.83 eV indicates a mechanism that requires two metastable He atoms for the formation of a cation, as proposed by Renzler et al. [41]. Thereby, at least $2 \times (z_f - z_i)$ metastable He atoms have to be formed to increase the charge state of a He droplet from z_i to z_f . The electrons emitted by the processes were as follows:



These electrons had kinetic energies in the order of 15 eV and thus were easily ejected from the droplets. Both the electrostatic interaction of electrons with multiply charged He droplets and the Coulomb energy required to accommodate additional charges in He droplets containing millions of He atoms were in the range of 0.1 eV and could not account for a slope of 1.66 eV.

At a hypothetical threshold energy, all projectile electrons have to escape after inelastic scattering and He* formation with essentially no excess kinetic energy, which becomes less probable for an increasing number of electrons. Thus, we propose that the unexpected increase of the appearance energy with increasing charging of He droplets (as seen in Figure 5) is simply related to the diminishing probability for the escape of large numbers of low-energy electrons.

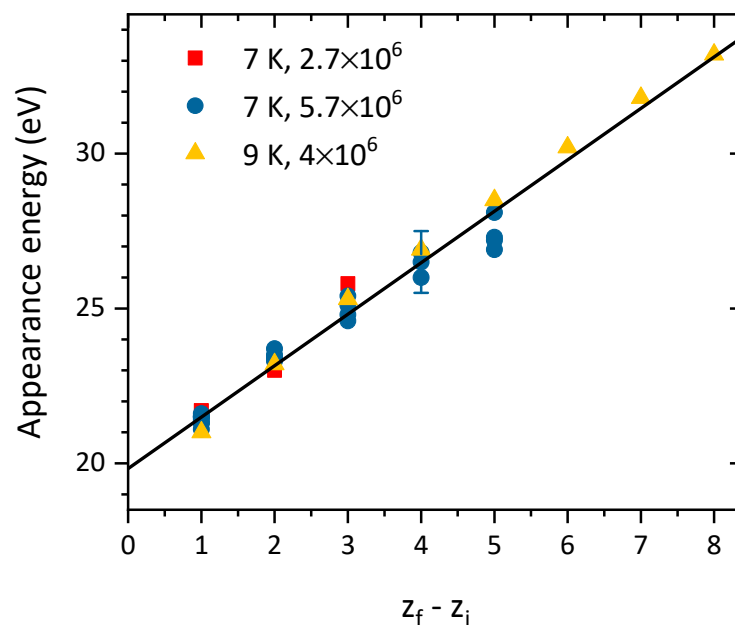


Figure 5. Appearance energies of the ion efficiency curves for electron ionization of positively charged He droplets, plotted as a function of the difference of the final and initial charge states $z_f - z_i$. Different symbols designate different expansion conditions and selected mass-per-charge values by the first energy analyzer. The black line is a linear fit to the data with a slope of 1.66 eV per removed electron. A general uncertainty of ± 1 eV for every threshold, determined by the vanishing current method, is plotted as a single error bar symbolically.

Figure 6a shows the ion efficiency curves for reactions that led to a reduction in the charge state of positively charged He droplets, having an initial mass-per-charge value of

5.7 million He atoms per charge. The corresponding reaction channels are found at relative m/z values larger than 1 in Figure 3. The color-coded curves are labeled with the ratio of the initial and final charge state z_i/z_f of the corresponding reaction channels in ascending values. In addition, the reaction channel that did not lead to a change in the charge state (designated as 1/1, the light gray line) is plotted with its corresponding y-axis at the right side of the diagram.

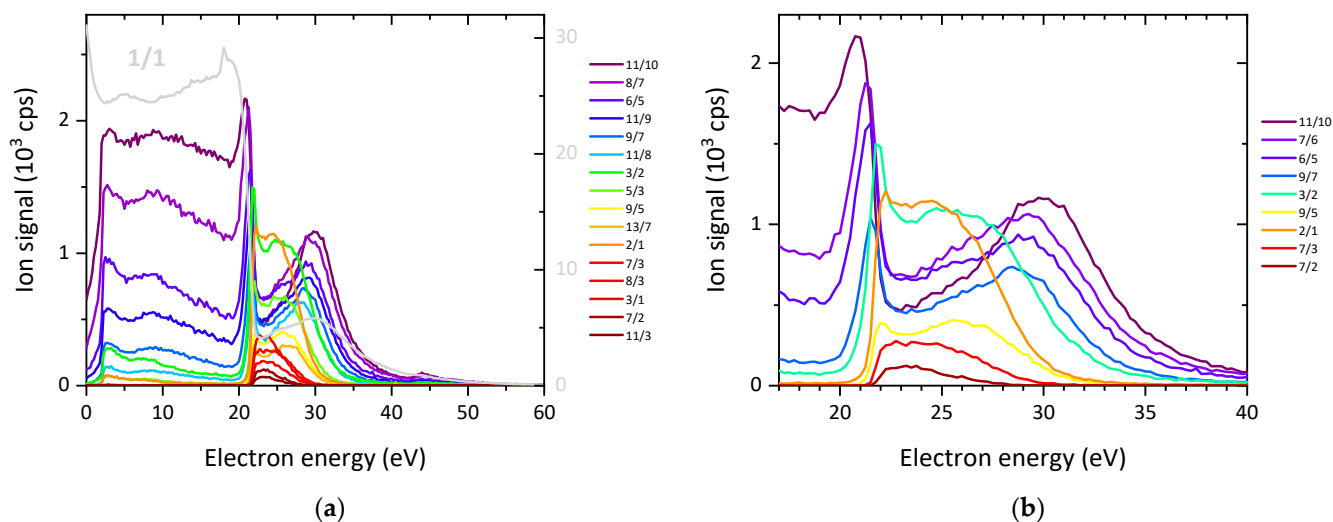


Figure 6. (a) Ion efficiency curves for electron capture of positively charged He droplets with a mass-per-charge ratio of 5.7 million He atoms per charge upon electron bombardment. The curves labels are sorted according to the ratio of the precursor to the final charge state. (b) Selection of every second data from (a), shown in more detail in the energy range around the 22 eV and 30 eV resonances.

The reduction of the charge state (i.e., the capture of the projectile electron) requires a minimum energy of about 2 eV, where a more- or less-pronounced resonance can be seen, followed by a second broad feature at around 10 eV and a narrow peak at around 22 eV, again followed by a broad peak at around 30 eV and a very weak resonance at around 44 eV. Table S2 in the Supplementary Materials lists the positions of these resonances for all ion efficiency curves measured for two different mass-per-charge values of the initially selected positively charged droplets. The ion efficiency curves for $m/z = 2.7$ million He atoms per charge are shown in the Supplementary Materials in Figure S3. Figure 6b shows the energy range between 17 eV and 40 eV in more detail.

According to Figure 7, the actual positions of the features around 22 eV and 30 eV seemed to depend on the ratio of the final and initial charge states. For both initially selected mass-per-charge values (designated by solid symbols for 2.7 and open symbols for 5.7 million He atoms per charge), the data followed the same nonlinear trend. The lines were allometric fits to the data of the form of

$$y = a + b \cdot x^c,$$

The fitting parameters were $a = 22.42$ (25.28), $b = -2.14$ (6.79) and $c = 3.25$ (3.28) for the two resonances, respectively.

Both resonance positions exhibited a smooth monotonic behavior. The low-energy resonance started at low z_f/z_i values of 22.5 eV and dropped with increasing z_f/z_i to less than 21 eV. In contrast, the high-energy resonance increased from 25 eV at $z_f/z_i = 0.2$ to 30 eV at $z_f/z_i = 0.9$. Both curves followed a similar power dependence with fit parameters $c = 3.25$ and 3.28 for the low- and high-energy resonances, respectively. Large z_f/z_i values corresponded to the single-electron capture of a highly charged He droplet, whereas small values were obtained when a highly charged droplet captured $z_i - 1$ electrons or a positively charged droplet was neutralized (i.e., $z_f = 0$). The values of 22.42 eV and 25.28 eV

for $z_f/z_i = 0$ indicate electronic excitation and threshold ionization of He atoms as potential underlying processes, respectively. The formation of He* as well as the formation of He⁺ additionally generated one or two low-energy electrons, respectively, which if trapped inside the droplet would reduce its charge state.

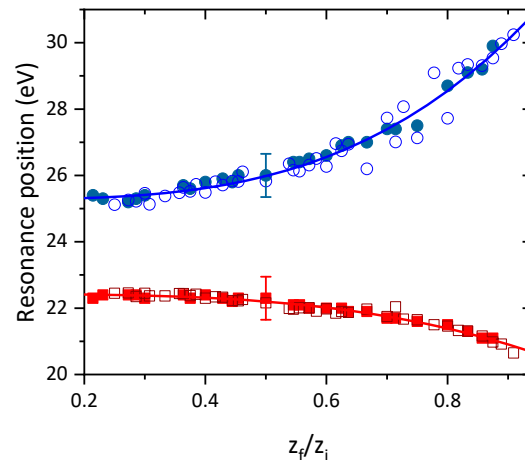


Figure 7. Positions of the resonances for charge reduction as a function of the ratio of the final and initial charge states, determined from the ion efficiency curves shown in Figure 6a,b. Bold symbols designate mass-per-charge values of the selected precursor droplets of 2.7 million He atoms per charge, and open symbols represent those of 5.7 million He atoms per charge. A general uncertainty of ± 0.65 eV for all resonance positions considering the spread in electron energy of the set-up is plotted as a single error bar for both resonances.

The charge centers of the multiply charged He droplets were located close to their surface [33], quite different from the highly charged water droplets [42,43]. The mass of a droplet scales with the cube of its radius, whereas the surface is only proportional to the square of the radius. Droplets with the same mass-per-charge values were selected by the energy analyzers. However, with the increasing charge state z , their surface charge densities rose with $z^{1/3}$. Thus, the energy gain of an electron due to the Coulomb attraction from charged droplets having the same mass-per-charge ratio was larger for droplets having a high initial charge state z_i , albeit with a larger radius. This explains qualitatively the lowering of the low-energy resonance to a value of 20.3 eV at $z_f/z_i = 1$, which was close to 19.8 eV for the formation of He in the 2^3S state. The high-energy resonance reached a value of 32 eV at $z_f/z_i = 1$, and a tentative explanation for this resonance is dissociative electron attachment to impurities, such as H₂O from the residual gas captured by large He droplets or H₂ impurities in the He gas used for the droplet formation. Both H₂O and H₂ exhibit resonances for dissociative electron attachment at about 10 eV when embedded in He droplets [44,45] and subsequent resonances upshifted by the energy required to form metastable He in droplets (i.e., $19.8 + 1.66 = 21.46$ eV). The probability for both impurities to be found in a droplet increased with the size of the droplet; in the case of water, it scaled with the geometric cross section that was proportional to the number of He atoms in the droplet to the power of $2/3$, and for hydrogen, it was proportional to the number of He atoms. Thus, highly charged droplets are inevitably prone to more impurities and exhibit more intense peaks at these electron energy ranges. However, as the droplets were already initially charged, we expect that these impurities are preferentially localized at the charge centers.

3.2.2. Total Cross Sections

For ionization (increase in the charge state, red line) and electron capture (decrease in charge state, blue line), we summed up all measured ion efficiency curves and plotted them in Figure 8 together with the channel that did not lead to a change in the charge state (light gray line). With the second ion source turned off, we recorded a signal of 40,000 cps. If only cationic

droplets were formed, the sum of all cationic product ions (black solid line in Figure 8) should have been a constant line at 40,000 cps. Two narrow resonances at 2 eV and 22 eV as well as a weaker feature at 44 eV could be assigned to neutralization or the formation of negatively charged droplets via electron capture and He^{*-} formation. At electron energies higher than 60 eV, a monotonic decrease of the sum of the cationic droplets was observed, which resulted from droplets having either a final charge state $z_f < 1$ (anions or neutral) or being very large (unresolved reaction channels to high charge states in Figure 3). Only reaction channels with $z_f/z_i \leq 6$ were recorded in the present study. Thus, a substantial part of the cationic products was missing which, according to Figure 4, was expected to have a maximum ion yield at electron energies larger than 80 eV. This readily explains the gradual loss of cationic product droplets at electron energies higher than 60 eV.

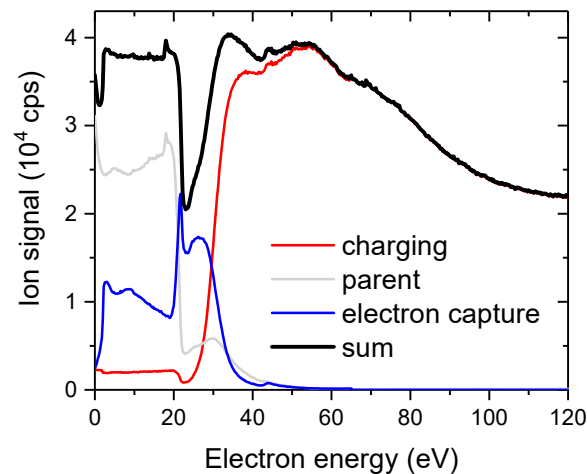


Figure 8. The sum of all ion efficiency curves measured for charging ($z_f > z_i$, red line) and electron capture ($z_f < z_i$, blue line) of positively charged He droplets with an initial mass-per-charge ratio of 5.7 million He atoms per charge. The light gray line represents the ion efficiency curve of the selected charged precursor droplets, and the bold black line is the sum of these three channels (i.e., the yield of all positively charged product ions).

In Figure 9, the loss of positively charged He droplets (40,000 cps minus the sum of all positively charged product ions, the black line in Figure 8) is plotted (black bold line) together with the anion efficiency curve for the formation of negatively charged He droplets upon electron irradiation of neutral droplets with an average size of 1.8 million He atoms [38] (blue line).

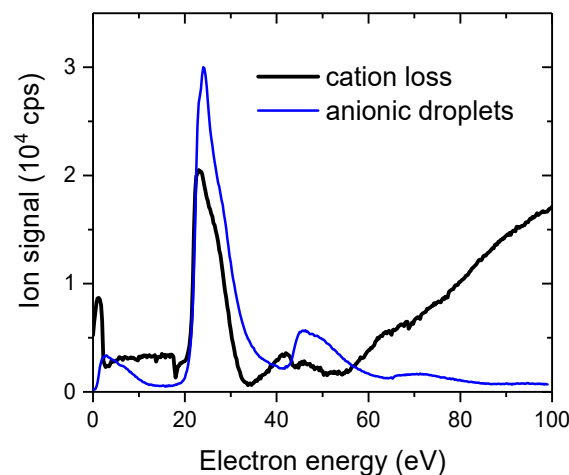


Figure 9. The loss of positively charged He droplets upon electron irradiation (black bold line) in comparison with the formation of negatively charged He droplets upon electron capture into neutral He droplets.

3.3. Anions to Cations

In this section, we will focus on the interaction of electrons with negatively charged He droplets that are formed upon electron bombardment of neutral He droplets at the same expansion conditions (7 K and 2 MPa, average droplet size of 11 million He atoms [38]) with an electron energy of 30 eV and an electron current of 430 μA . The first energy filter (Analyzer 1 in Figure 1) selected a narrow slice of a log-normal-shaped distribution at a relative m/z of 3.2×10^7 He atoms per charge (corresponding to a relative m/z value of 1 in Figure 10a). In the second ion source (IS 2 in Figure 1), the selected droplets were crossed with a 175- μA electron beam and an electron energy of 60 eV. The contribution of multiply charged precursor droplets was very low, although only 4 million He atoms were sufficient to stabilize two negatively charged ionic centers [34]. Plotting the curve versus the reciprocal of the relative m/z value led to peaks centered at the corresponding charge state of the product ions (Figure 10b). Individual peaks could be resolved in this figure up to $z = 27$.

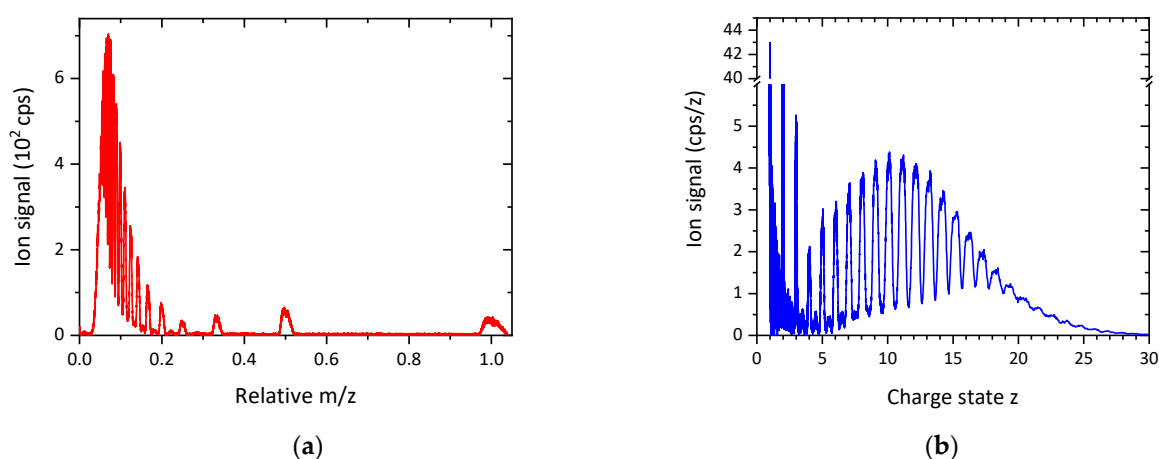


Figure 10. (a) Charge distributions of positively charged He droplets resulting from electron bombardment of mass-per-charge selected, negatively charged He droplets containing 32 million He atoms per charge. The electron energy of the second ion source (IS 2 in Figure 1) was set to 60 eV at an electron current of 175 μA . (b) The same data plotted as a function of the reciprocal of m/z , exhibiting pronounced peaks at integer values of z up to $z = 27$.

3.3.1. Ion Efficiency Curves

Ion efficiency curves for the formation of cationic He droplets upon electron ionization of negatively charged precursors containing 12 million He atoms per charge are plotted in Figure 11. The left diagram (a) contains data upon electron ionization of a singly charged anionic helium droplet, and the right diagram (b) shows data of a doubly charged anionic helium droplet. The conversion of anions into cations requires a certain amount of energy to remove at least two electrons from a large droplet. Penning ionization of He^{*-} , as described by Renzler et al. [41], would be a possible mechanism, as well as direct ionization of a He atom of the droplets. In both cases, the electrons require enough kinetic energy to escape the Coulomb attraction by the now positively charged droplets.

3.3.2. Appearance Energies

Via the vanishing current method, the threshold energies were determined with an uncertainty of ± 1 eV for all reaction channels measured at two initial mass-per-charge values of -12 and -32 million (shown in the Supplementary Materials, Figure S4) He atoms per charge, and the values are summarized in Table S3 and plotted in Figure 12 as a function of the final charge state z_f of the resulting cationic droplets. In contrast to the cations shown in Figure 5, the x-axis corresponds to the final charge state and not the difference $z_f - z_i$. Again, we assigned a slope of the fit of 1.34 eV to the decreasing probability of the ejection of an increasing number of low-energy electrons. The only

difference with the initially positively charged droplets (shown in Figure 5) was the fact that the appearance energies did not seem to depend on the initial charge state. The repulsive Coulomb interaction between the electrons and the initially negatively charged He droplets supported the escape of low-energy electrons. However, we were only able to obtain data for $z_i = -1$ and -2 .

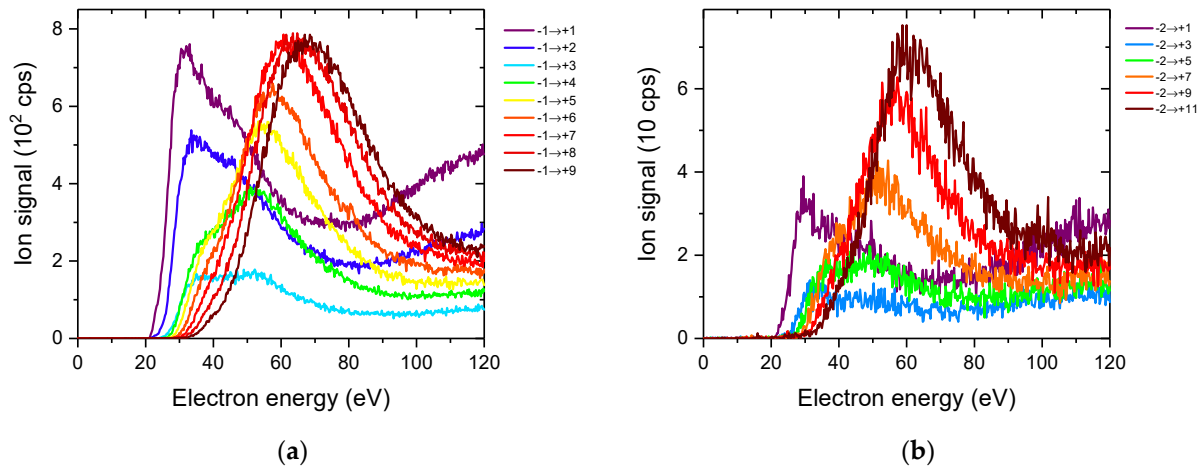


Figure 11. (a) Ion efficiency curves for electron ionization of negative singly charged He droplets with a mass-per-charge ratio of 12 million He atoms per charge. The curves are sorted according to the final charge states of the resulting positively charged droplets. (b) Ion efficiency curves for the formation of positively charged He droplets upon electron ionization doubly charged anionic He droplets containing 24 million He atoms.

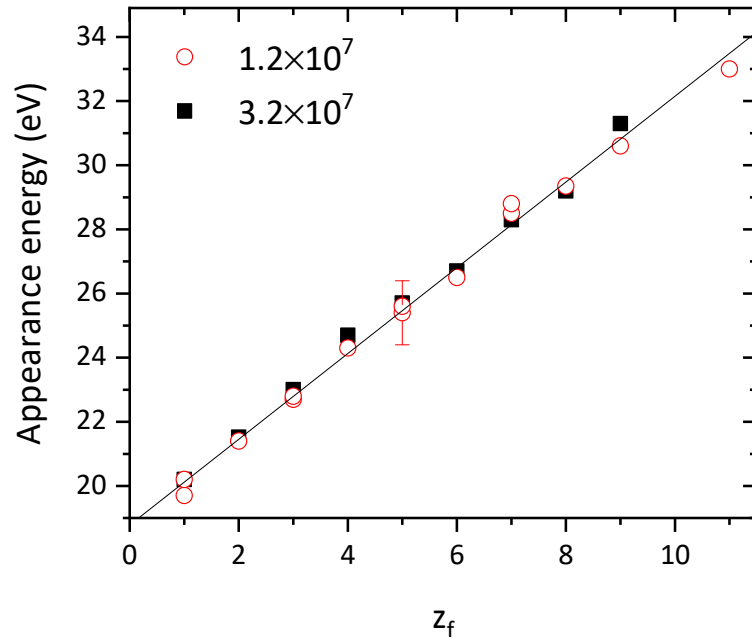


Figure 12. Appearance energies of the ion efficiency curves for electron ionization of negatively charged He droplets and the formation of cations, plotted as a function of the final charge states z_f of the positively charged product droplet for two He droplet source temperatures (12 and 32 million He atoms per charge, designated as open circles and filled squares, respectively). The black line is a linear fit to the data with a slope of 1.34 eV per removed electron. A general uncertainty of ± 1 eV that applies to every threshold, determined by the vanishing current method, is represented by a single error bar.

3.4. Anions to Anions

The ion efficiency curve for the attachment of an electron to an already negatively charged droplet is shown exemplarily for a triply charged anionic He droplet containing 120 million He atoms in Figure 13. This process proceeded via two narrow resonances located at 3 eV and 22 eV, and above 30 eV, an almost linear rise of the ion efficiency curve is observed. At these energies, He^+ was likely formed, and the net charge would be reduced if both the projectile and secondary electron were trapped in the large He droplet having a diameter of 220 nm. This increase of negative charging at electron energies higher than 30 eV was expected to be one of the loss channels for cationic He droplets mentioned in Section 3.2.2.

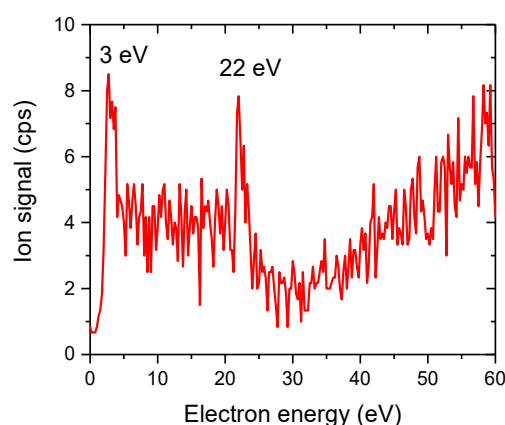


Figure 13. Anion efficiency curve for the single electron capture of a triply charged anionic He droplet containing 120 million He atoms. The process is preferentially operational at two narrow resonances of 3 eV and 22 eV.

4. Conclusions

The interaction of electrons with mass-per-charge-selected He droplets containing millions of He atoms was studied in detail. Ion efficiency curves were determined for individual reaction channels that could be assigned to the removal or addition of electrons. In contrast to the single-collision conditions typically used for electron scattering experiments with molecular or atomic targets, the huge geometric cross section of the investigated helium droplets and the high electron currents chosen in the present study ensured multi-collision conditions, with up to several hundred electron hits per droplet. As was already reported previously [33,34], the mass loss due to neutral He evaporation or asymmetric Coulomb explosion was negligible, and so the interaction of electrons with large He droplets essentially only changed their charge states. Individual relative cross section curves for charging positively charged He droplets clearly showed that with increasing electron energy product, the droplets were preferentially ending up in higher charge states. Threshold energies at 22 eV and intensity anomalies in several ion efficiency curves demonstrate that metastable He formation is an important mechanism at all electron energies, since the cross section for electron ionization of He^* is almost 20 times larger than that of ground state helium [37]. The total cross section for ionization exhibited a steep increase from 25 eV to 35 eV, followed by a gentle rise up to 70 eV and an exponential decrease at higher electron energies. The latter we explained with ionization into highly charged droplets that could not be assigned in the present experiments. In the case of electron capture, low-energy electrons can be directly trapped, preferentially with kinetic energies around 2 eV or after inelastic scattering and He^* formation at 22 eV and, to a less extent, at 44 eV. At these electron energies, we observed the loss of positively charged He droplets into neutral or negatively charged products.

Some results obtained in the present study for He droplets may also hold for droplets and nanoparticles made of other atoms and molecules, such as water. In that case, similar

experiments could provide valuable insight into the radiation physics and chemistry of water as well as the initial processes happening in electrospray ionization.

Supplementary Materials: The Supplementary Materials containing tables and additional figures referenced in the results and discussion section is available online at <https://www.mdpi.com/article/10.3390/atoms9040074/s1>.

Author Contributions: Conceptualization, F.L. and P.S.; methodology, formal analysis, and data curation, F.L.; writing—original draft preparation, P.S.; writing—review and editing, F.Z., E.G., F.L. and P.S.; funding acquisition, E.G. and P.S. All authors have read and agreed to the published version of the manuscript.

Funding: Open Access Funding by the European Region Fund, Project No EFRE 2016-4, and Open Access Funding by the Austrian Science Fund (FWF), grant number T1181.

Data Availability Statement: The data presented in this work are available from the corresponding author upon reasonable request.

Conflicts of Interest: The authors declare no conflict of interest.

References

1. Janev, R.K.; Reiter, D. Collision processes of CH_y and CH_y⁺ hydrocarbons with plasma electrons and protons. *Phys. Plasmas* **2002**, *9*, 4071–4081. [[CrossRef](#)]
2. McCall, B.J.; Huneycutt, A.J.; Saykally, R.; Geballe, T.R.; Djuric, N.; Dunn, G.H.; Semaniak, J.; Novotny, O.; Al-Khalili, A.; Ehlerding, A.; et al. An enhanced cosmic-ray flux towards ζ Persei inferred from a laboratory study of the H₃⁺–e[−] recombination rate. *Nature* **2003**, *422*, 500–502. [[CrossRef](#)] [[PubMed](#)]
3. Deutsch, H.; Becker, K.; Probst, M.; Märk, T.D. The Semiempirical Deutsch-Märk Formalism: A Versatile Approach for the Calculation of Electron-Impact Ionization Cross Sections of Atoms, Molecules, Ions, and Clusters. In *Advances in Atomic, Molecular, and Optical Physics*; Arimondo, E., Berman, P.R., Lin, C.C., Eds.; Elsevier: Amsterdam, The Netherlands, 2009; Volume 57, pp. 87–155.
4. Kim, Y.; Irikura, K.; Ali, M. Electron-impact total ionization cross sections of molecular ions. *J. Res. Natl. Inst. Stand. Technol.* **2000**, *105*, 285–291. [[CrossRef](#)] [[PubMed](#)]
5. Uddin, M.; Basak, A.K.; Islam, A.K.M.; Malik, F.B. Electron impact single ionization of light ionic targets with charge $q > 2$. *J. Phys. B* **2004**, *37*, 1909–1922. [[CrossRef](#)]
6. Pindzola, M.S.; Robicheaux, F.; Colgan, J. Electron-impact ionization of H+2 using a time-dependent close-coupling method. *J. Phys. B* **2005**, *38*, L285–L290. [[CrossRef](#)]
7. Peart, B.; Dolder, K.T. Collisions between electrons and H₂⁺ ions. IV. Measurements of cross sections for dissociative ionization. *J. Phys. B* **1973**, *6*, 2409–2414. [[CrossRef](#)]
8. Müller, A.; Tinschert, K.; Achenbach, C.; Salzborn, E.; Becker, R. A new technique for the measurement of ionization cross sections with crossed electron and ion beams. *Nucl. Instrum. Methods Phys. Res. Sect. B* **1985**, *10–11*, 204–206. [[CrossRef](#)]
9. Defrance, P.; Brouillard, F.; Claeys, W.; Van Wassenhove, G. Crossed beam measurement of absolute cross sections: An alternative method and its application to the electron impact ionisation of He⁺. *J. Phys. B* **1981**, *14*, 103–110. [[CrossRef](#)]
10. Belic, D.S.; Ristic, M.M.; Cherkani-Hassani, H.; Urbain, X.; Defrance, P. Electron-impact dissociation of N₂D⁺ cations to D⁺ fragments. *Eur. Phys. J. D* **2020**, *74*, 1–8. [[CrossRef](#)]
11. Dolder, K.T.; Peart, B. Collisions between electrons and ions. *Rep. Prog. Phys.* **1976**, *39*, 693–749. [[CrossRef](#)]
12. Matt, S.; Echt, O.; Rauth, T.; Dünser, B.; Lezius, M.; Stamatovic, A.; Scheier, P.; Märk, T.D. Electron impact ionization and dissociation of neutral and charged fullerenes. *Z. Phys. D* **1997**, *40*, 389–394. [[CrossRef](#)]
13. Scheier, P.; Hathiramani, D.; Arnold, W.; Huber, K.; Salzborn, E. Multiple Ionization and Fragmentation of Negatively Charged Fullerene Ions by Electron Impact. *Phys. Rev. Lett.* **2000**, *84*, 55–58. [[CrossRef](#)]
14. Hathiramani, D.; Aichele, K.; Arnold, W.; Huber, K.; Salzborn, E.; Scheier, P. Electron-Impact Induced Fragmentation of Fullerene Ions. *Phys. Rev. Lett.* **2000**, *85*, 3604–3607. [[CrossRef](#)]
15. Becker, E.W.; Klingelhöfer, R.; Lohse, P. Notizen: Strahlen aus kondensiertem Helium im Hochvakuum. *Z. Nat. A* **1961**, *16*, 1259. [[CrossRef](#)]
16. Scheidemann, A.; Toennies, J.P.; Northby, J.A. Capture of neon atoms by He₄ clusters. *Phys. Rev. Lett.* **1990**, *64*, 1899–1902. [[CrossRef](#)]
17. Goyal, S.; Schutt, D.L.; Scoles, G. Vibrational spectroscopy of sulfur hexafluoride attached to helium clusters. *Phys. Rev. Lett.* **1992**, *69*, 933–936. [[CrossRef](#)]
18. Goyal, S.; Schutt, D.L.; Scoles, G. Infrared spectroscopy in highly quantum matrixes: Vibrational spectrum of sulfur hexafluoride ((SF₆)_{n=1,2}) attached to helium clusters. *J. Phys. Chem.* **1993**, *97*, 2236–2245. [[CrossRef](#)]
19. Hartmann, M.; Miller, R.E.; Toennies, J.P.; Vilesov, A. Rotationally Resolved Spectroscopy of SF₆ in Liquid Helium Clusters: A Molecular Probe of Cluster Temperature. *Phys. Rev. Lett.* **1995**, *75*, 1566–1569. [[CrossRef](#)]

20. Callegari, C.; Lehmann, K.K.; Schmied, R.; Scoles, G. Helium nanodroplet isolation rovibrational spectroscopy: Methods and recent results. *J. Chem. Phys.* **2001**, *115*, 10090. [[CrossRef](#)]
21. Toennies, J.P.; Vilesov, A.F. Superfluid Helium Droplets: A Uniquely Cold Nanomatrix for Molecules and Molecular Complexes. *Angew. Chem. Int. Ed.* **2004**, *43*, 2622–2648. [[CrossRef](#)]
22. Choi, M.Y.; Douberly, G.E.; Falconer, T.M.; Lewis, W.K.; Lindsay, C.; Merritt, J.M.; Stiles, P.L.; Miller, R.E. Infrared spectroscopy of helium nanodroplets: Novel methods for physics and chemistry. *Int. Rev. Phys. Chem.* **2006**, *25*, 15–75. [[CrossRef](#)]
23. Stienkemeier, F.; Lehmann, K. Spectroscopy and dynamics in helium nanodroplets. *J. Phys. B* **2006**, *39*, R127–R166. [[CrossRef](#)]
24. Northby, J.A. Experimental studies of helium droplets. *J. Chem. Phys.* **2001**, *115*, 10065. [[CrossRef](#)]
25. Callicoatt, B.E.; Förde, K.; Ruchti, T.; Jung, L.; Janda, K.C.; Halberstadt, N. Capture and ionization of argon within liquid helium droplets. *J. Chem. Phys.* **1998**, *108*, 9371–9382. [[CrossRef](#)]
26. Mauracher, A.; Echt, O.; Ellis, A.; Yang, S.; Bohme, D.; Postler, J.; Kaiser, A.; Denifl, S.; Scheier, P. Cold physics and chemistry: Collisions, ionization and reactions inside helium nanodroplets close to zero K. *Phys. Rep.* **2018**, *751*, 1–90. [[CrossRef](#)]
27. Tiggesbäumker, J.; Stienkemeier, F. Formation and properties of metal clusters isolated in helium droplets. *Phys. Chem. Chem. Phys.* **2007**, *9*, 4748–4770. [[CrossRef](#)] [[PubMed](#)]
28. Atkins, K.R. *Course XXI on Liquid Helium, Proceedings of International School of Physics Enrico Fermi, New York*; Careri, G., Ed.; Academic Press: New York, NY, USA, 1963; pp. 403–413.
29. Halberstadt, N.; Janda, K.C. The resonant charge hopping rate in positively charged helium clusters. *Chem. Phys. Lett.* **1998**, *282*, 409–412. [[CrossRef](#)]
30. Ellis, A.M.; Yang, S. Model for the charge-transfer probability in helium nanodroplets following electron-impact ionization. *Phys. Rev. A* **2007**, *76*, 032714. [[CrossRef](#)]
31. Atkins, K.R. Ions in Liquid Helium. *Phys. Rev.* **1959**, *116*, 1339–1343. [[CrossRef](#)]
32. Mateo, D.; Eloranta, J. Solvation of Intrinsic Positive Charge in Superfluid Helium. *J. Phys. Chem. A* **2014**, *118*, 6407–6415. [[CrossRef](#)]
33. Laimer, F.; Kranabetter, L.; Tiefenthaler, L.; Albertini, S.; Zappa, F.; Ellis, A.M.; Gatchell, M.; Scheier, P. Highly Charged Droplets of Superfluid Helium. *Phys. Rev. Lett.* **2019**, *123*, 165301. [[CrossRef](#)]
34. Laimer, F.; Zappa, F.; Scheier, P.; Gatchell, M. Multiply Charged Helium Droplet Anions. *Chem.—A Eur. J.* **2021**, *27*, 7283–7287. [[CrossRef](#)]
35. Laimer, F.; Zappa, F.; Scheier, P. Size and Velocity Distribution of Negatively Charged Helium Nanodroplets. *J. Phys. Chem. A* **2021**, *125*, 7662–7669. [[CrossRef](#)]
36. Krishna, M.V.R.; Whaley, K.B. Wave functions of helium clusters. *J. Chem. Phys.* **1990**, *93*, 6738–6751. [[CrossRef](#)]
37. Bogdanov, E.; Demidov, V.; Kaganovich, I.D.; Koepke, M.E.; Kudryavtsev, A. Modeling a short dc discharge with thermionic cathode and auxiliary anode. *Phys. Plasmas* **2013**, *20*, 101605. [[CrossRef](#)]
38. Gomez, L.F.; Loginov, E.; Sliter, R.; Vilesov, A.F. Sizes of large He droplets. *J. Chem. Phys.* **2011**, *135*, 154201. [[CrossRef](#)]
39. Matt, S.; Dünser, B.; Lezius, M.; Deutsch, H.; Becker, K.; Stamatovic, A.; Scheier, P.; Märk, T.D. Absolute partial and total cross-section functions for the electron impact ionization of C60 and C70. *J. Chem. Phys.* **1996**, *105*, 1880–1896. [[CrossRef](#)]
40. Mauracher, A.; Daxner, M.; Postler, J.; Huber, S.E.; Denifl, S.; Scheier, P.; Toennies, J.P. Detection of Negative Charge Carriers in Superfluid Helium Droplets: The Metastable Anions He^{*-} and He₂^{*-}. *J. Phys. Chem. Lett.* **2014**, *5*, 2444–2449. [[CrossRef](#)]
41. Renzler, M.; Daxner, M.; Weinberger, N.; Denifl, S.; Scheier, P.; Echt, O. On subthreshold ionization of helium droplets, ejection of He⁺, and the role of anions. *Phys. Chem. Chem. Phys.* **2014**, *16*, 22466–22470. [[CrossRef](#)]
42. Kwan, V.; Consta, S. Molecular Characterization of the Surface Excess Charge Layer in Droplets. *J. Am. Soc. Mass Spectrom.* **2020**, *32*, 33–45. [[CrossRef](#)]
43. Kwan, V.; Malevanets, A.; Consta, S. Where Do the Ions Reside in a Highly Charged Droplet? *J. Phys. Chem. A* **2019**, *123*, 9298–9310. [[CrossRef](#)]
44. Zappa, F.; Denifl, S.; Mähr, I.; Bacher, A.; Echt, O.; Märk, T.D.; Scheier, P. Ultracold Water Cluster Anions. *J. Am. Chem. Soc.* **2008**, *130*, 5573–5578. [[CrossRef](#)]
45. Renzler, M.; Kuhn, M.; Mauracher, A.; Lindinger, A.; Scheier, P.; Ellis, A.M. Anionic Hydrogen Cluster Ions as a New Form of Condensed Hydrogen. *Phys. Rev. Lett.* **2016**, *117*, 273001. [[CrossRef](#)]